JOURNAL OF MATERIALS SCIENCE **38** (2003) 2901 – 2906

Preparation and electrochemical characterization of Sr- and Mn-doped $LaGaO_3$ as anode materials for LSGM-based SOFCs

QINGXI FU, XINGYAN XU, DINGKUN PENG, XINGQIN LIU, GUANGYAO MENG*
Department of Materials Science & Engineering, University of Science and Technology of China, Hefei 230026, Anhui, People's Republic of China
E-mail: mgym@ustc.edu.cn

Sr- and Mn-doped lanthanum gallate powders (LSGMn, $La_{0.9}Sr_{0.1}Ga_{1-x}Mn_xO_{3-\delta}$, $x = 0.20$, 0.35, 0.43) were prepared by glycine-nitrate combustion synthesis. X-ray diffraction patterns indicate the perovskite structure was formed without any second phase after calcining the powders at 1000°C for 4 h. Compacts of powders synthesized under stoichiometric combustion were sintered to densities over 95% of theoretical values. The electrical conductivity of this material in both air and H_2 were characterized using AC impedance spectroscopy. It showed that the conductivity in H_2 atmosphere is lower than that in air due to p-type electrical conduction in this material, and the electrical conductivity increases remarkably with increasing manganese content. Good chemical stability of $La_{0.9}Sr_{0.1}Ga_{1-x}Mn_xO_{3-\delta}$ in H_2 atmosphere as well as the relatively high conductivity makes it an appropriate anode material for Sr- and Mg-doped lanthanum gallate (LSGM)-based IT-SOFCs. Preliminary fuel cell performance measurements were performed, showing promising electrochemical properties of such anode materials.

1. Introduction

In recent years, strontium- and magnesium-doped lanthanum gallate perovskite oxide (LSGM) has been widely investigated as electrolyte material for intermediate temperature (IT) solid oxide fuel cells (SOFCs) due to its relatively high and pure ionic conductivity [1–8]. Compared to high temperature SOFCs based on YSZ electrolytes, the performance of IT-SOFCs depends more on the electrode-electrolyte interfaces, since the interfacial polarization of a solid-state cell increases rapidly as the operating temperature is reduced [9]. In LSGM-based SOFCs, the most widely used anode materials are Ni-based materials, including metallic Ni, Ni-LSGM cermets [10, 11], Ni-doped ceria (DCO) cermets [11, 12]. It was found that Ni could react with LSGM and formed poor-conductive $LaNiO_3$-based oxides or $LaSrGa(Ni)O_{4-\delta}$ at the electrolyte/anode interface, which increased rapidly the anode polarization [10, 11]. Huang *et al.* [2] used DCO buffer layer to prevent the direct contact of Ni with LSGM, and improved the fuel cell performance successfully. However, later investigation found that even DCO could react with LSGM at high temperatures (>1150°C), forming another kind of poor-conductive oxide, $SrLaGa_3O_7$ (800°C, 10^{-6} S cm^{-1}) [10, 13]. Therefore, it is necessary to search for other new anode materials, which show both good chemical/physical compatibility with the LSGM electrolyte and high catalytic activity towards fuel oxidation reaction.

It is well known that Ni-based anode materials can cause carbon-deposition problem when hydrocarbon fuels are used because Ni has relatively high catalytic activity towards the splitting decomposition of hydrocarbon molecules. In contrast, most oxides do not favor the carbon-formation reaction [14]. Therefore, replacing traditional Ni-based cermet anode with oxides would avoid the carbon-deposition problem. On the other hand, good anode materials require both high electronic conductivity and as high ionic conductivity as possible, and oxides with such properties are called mixed ionic/electronic conductors (MIECs). Lanthanum gallates doped with transition metal elements are good MIECs [7, 9, 15–17]. Thus, the use of these MIECs as anode materials for LSGM-based SOFCs offers at least three advantages. Firstly, they are compatible both chemically and physically with LSGM electrolytes, minimizing interfacial reactions due to inter-diffusion or chemical reaction. Secondly, they should have thermal expansion coefficients similar to that of LSGM, minimizing thermally induced stresses at the interface during thermal cycling and, thus improving adhesion of the electrode to the electrolyte. Thirdly, they would avoid the carbon-deposition problem, as discussed above.

*Author to whom all correspondence should be addressed.

Due to the strong reducing atmosphere at the anode chamber, one important requirement for anode materials is the good stability under reducing atmosphere. Among the transition metal doped lanthanum gallates, most of them have bad chemical stability in reducing atmosphere [9, 18–20], which makes them inappropriate for anode materials. One material, 10 mol% Sr- and 20 mol% Mn-doped lanthanum gallate, $La_{0.9}Sr_{0.1}Ga_{0.8}Mn_{0.2}O_{3-\delta}$ was reported to have good chemical stability and ever used as anode materials for LSGM-based SOFCs [9]. However, due to low transition metal dopant concentration (only 20 mol%), the material exhibits mainly ionic conduction and the whole electrical conductivity is relatively low [9]. Since the conductivity of transition metal doped lanthanum gallate increases with increasing transition metal doping [7], we propose to improve the conductivity of LSGMn by increasing Mn content. If the conductivity is increased without the loss of chemical stability, the higher manganese doped lanthanum gallate may be used as a good anode material for LSGM-based IT-SOFCs.

In this paper, we reported the preparation of Sr- and Mn-doped lanthanum gallate powders ($La_{0.9}Sr_{0.1}Ga_{1-x}Mn_xO_{3-\delta}$, $x = 0.2$, 0.35, 0.43) by a glycine-nitrate process (GNP). The GNP is a self-combustion method using glycine as fuel and the nitrates of metal components of the material to be synthesized as oxidants. It can prepare a high specific surface powder with single-phase composition in very short time. It is especially appropriate for the fabrication of multi-component system such as doped perovskite compounds [21, 22]. The temperature and atmosphere dependence of the electrical conductivity of sintered pellets from as-prepared powders, as well as their chemical stability under H_2 atmosphere were also characterized. In addition, the fuel cell performance with such LSGMn anodes was presented.

2. Experiment

2.1. Sample synthesis

The super fine powders with composition of $La_{0.9}Sr_{0.1}Ga_{1-x}Mn_xO_{3-\delta}$ ($x = 0.20$, 0.35, 0.43) were synthesized by GNP. The starting materials were glycine (as the fuel), La-, Sr-, Ga- and Mn nitrates (as oxidants). The glycine was added into the mixed nitrate solution in a molar ratio of 1:1 for fuel: oxidant (stoichiometric combustion). The mixed solutions were heated until sufficient water was removed for combustion to occur. The resulting ash was pre-calcined at 350°C in air for 2 h to remove residual organic substances. Subsequent calcinations were performed at 1000°C in air. The calcined powders were compacted in a steel die and sintered at 1500°C for 4 h. The densities of the sintered pellets were measured by the Archimedes method. Phase development was determined by X-ray diffraction (XRD) analysis using Cu K_α radiation (MXP18AHF, Mac Science Co. Ltd.).

2.2. Microstructure

The morphology or microstructure of powders and well-polished pellets was observed with TEM (H-800) and SEM (Hitachi X-650). Au coating was applied on the surfaces or fracture surfaces to prevent charging before observation and photo-taken.

2.3. Electrical conductivity

The conductivity of sintered pellets was obtained from two-probe impedance spectroscopy. Platinum electrodes were applied on both surfaces of pellets by coating platinum paste and then firing at 850°C for 0.5 h. Measurements were made with an computer-interfaced impedance analyzer (GenRad 1689 Precision RLC Digibridge) over a frequency range of 12–10^5 Hz in the temperature range of 500°C–800°C. The effect of Pt lead on the resistance was removed through carefully zeroing before measurement. Each sample was measured in air and H_2 atmosphere, respectively.

2.4. Chemical stability in reducing atmosphere

The sintered pellets were exposed to H_2 at 750°C for 5 h, followed by XRD measurement and SEM observation to examine whether there is any change on both phase structure and microstructure after heat treatment in strong reducing atmosphere.

2.5. Fuel cell performance

To evaluate the performance of LSGMn anodes, fuel cells were constructed and measured. The powder of electrolyte material, $La_{0.9}Sr_{0.1}Ga_{0.8}Mg_{0.2}O_{2.85}$, was prepared by GNP, and the dense electrolyte disks were obtained by sintering the compacts of the powder at 1500°C for 5 h in air. The cathode material is commercial $La_{0.6}Sr_{0.4}Co_{0.2}Fe_{0.8}O_3$ powder (LSCF, Seattle Specialty). Both electrodes were applied by screen-printing technique. The sintering temperatures for LSGMn anode and LSCF cathode are 1350°C and 1200°C, respectively. The anode was first applied and sintered to avoid the densification of the cathode. Platinum anode was also used as a comparison. It was prepared by paste-painting followed by sintering at 850°C for one hour after the cathode was finished. All the fuel cells fabricated have the same electrolyte thickness of 0.8 mm. The heat treatment processes of electrodes for different cells are the same except for the Pt electrodes. In addition, the fuel cell performances were measured at the same conditions (e.g., gas flow, temperature, etc.). The fuel gas was wet H_2 (containing 3% water vapor) and the oxidant gas was O_2. Therefore, it is reasonable to believe that the difference in fuel cell performance will reflect the difference in anode performance.

3. Results and discussion

In this paper, $La_{0.9}Sr_{0.1}Ga_{1-x}Mn_xO_{3-\delta}$ compositions are designated by the abbreviation LSGMn. The numbers following the abbreviation refer to the relative proportions of Sr and Mn in the material. For example, $La_{0.9}Sr_{0.1}Ga_{0.8}Mn_{0.2}O_{2.85}$ is designated LSGMn-1020.

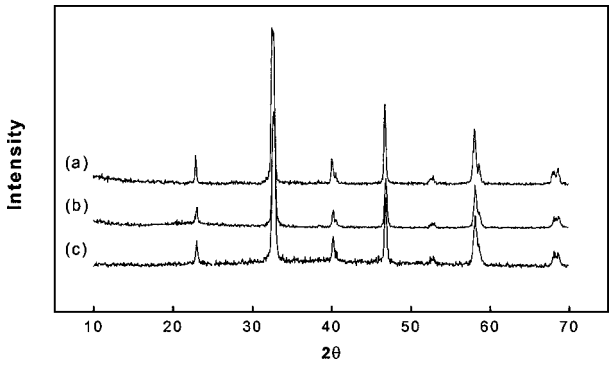

Figure 1 X-ray diffraction patterns of powders produced by GNP, calcined at 1000°C: (a) LSGMn-1020, (b) LSGMn-1035, and (c) LSGMn-1043.

3.1. Phase development

The results of the X-ray diffraction patterns for the LSGMn-1020, LSGMn-1035 and LSGMn-1043 are shown in Fig. 1. It can be seen that all powders with different manganese contents produced by "stoichiometric" combustion followed by calcination at 1000°C for 4 h exhibited almost pure pervoskite structure. Compared with the traditional solid state reaction, by which the perovskite formation temperature is usually above 1300°C, and often with impure second phases, the glycine-nitrate process can remarkably lower the phase formation temperature. In the glycine-nitrate process, the glycine functions not only as a fuel, but also as a complexing agent. One end of the glycine molecule, the amine group ($-NH_2$), can complex with the transitional metal ions, and the other end of the glycine molecule, the carboxyl group ($-COO$), can complex with alkaline earth metal ions. Because La^{3+} ionic radius and chemical properties are similar to that of alkaline earth metal ions, it would also complex with carboxyl group. The complexation could prevent individual components from precipitation before combustion process, resulting in homogeneous products and lower phase formation temperature.

3.2. Microstructure

TEM microphoto for GNP-prepared powders calcined at 1000°C is shown in Fig. 2. It can be found that the powder is fine and homogeneous, with the mean particle size of around 100 nm. The fine and homogeneous powder would have high sinterability. SEM photographs of the surfaces of the sintered samples are shown in Fig. 3A. The surface microstructure reveals uniform and fine grain growth about 2–3 μm. No pore was observed on the surface of the sample, but there were some pores from the fracture surface of the sample, as shown in Fig. 3C. According to the measurement (Archimedes method), the sintered density is 6.6 g/cm^3, which is about 95% of the theoretical value.

3.3. Electrical conductivity

Figs 4 and 5 show the impedance spectra of LSGMn-1020 and LSGMn-1035 at different atmospheres and temperatures. It can be found that the impedance spectra

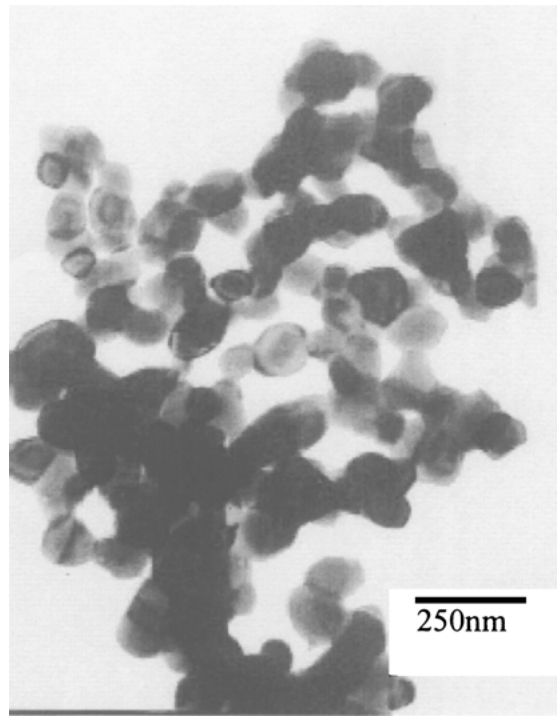

Figure 2 TEM micrograph of LSGMn powder calcined at 1000°C.

for samples with the same Mn content appeared similar in air and H_2 atmospheres. However, the spectra for samples with different Mn content appeared quite different. For LSGMn-1020, the spectra contain one straight line and one semi-circle, but the spectra for LSGMn-1035 contain only one straight line perpendicular to the real axis. The spectra of LSGMn-1043 have similar shapes with that of LSGMn-1035, i.e., also straight lines, so they are not shown here. The differences in spectra indicate different electrical conduction mechanisms. For LSGMn-1020, ionic conduction dominates [9]. In contrast, as the Mn content increases, p-types electronic conduction increases gradually. Thus, the p-type electronic conduction dominates for LSGMn-1035 and LSGMn-1043.

Assuming the equivalent circuit of the semi-circle in Fig. 4 is the parallel combination of a resistance (R) and capacitance (C), the capacitance of the component can be obtained according to the following equation,

$$C = \frac{1}{2\pi f^* R} \tag{1}$$

where R is the radius of the semi-circle and f^* is the relaxation frequency of the component (corresponding to the apex of the semi-circle).

The fitted C value in Fig. 4 (in air) is at the range of 200–300 μF, and it is even larger ($>$1000 μF) for spectra in H_2 atmosphere. So large C values indicate that the semi-circle would be attributed to the interfacial double layer capacitance. For ionic conductive electrolyte, the Pt electrode acts as a blocking electrode, resulting in the appearance of double layer capacitance. In contrast, for electrolyte predominated by p-type electronic conduction, this blocking effect disappears and so no semi-circle is observed in the impedance spectra. The resistance of the electrolyte was determined from the

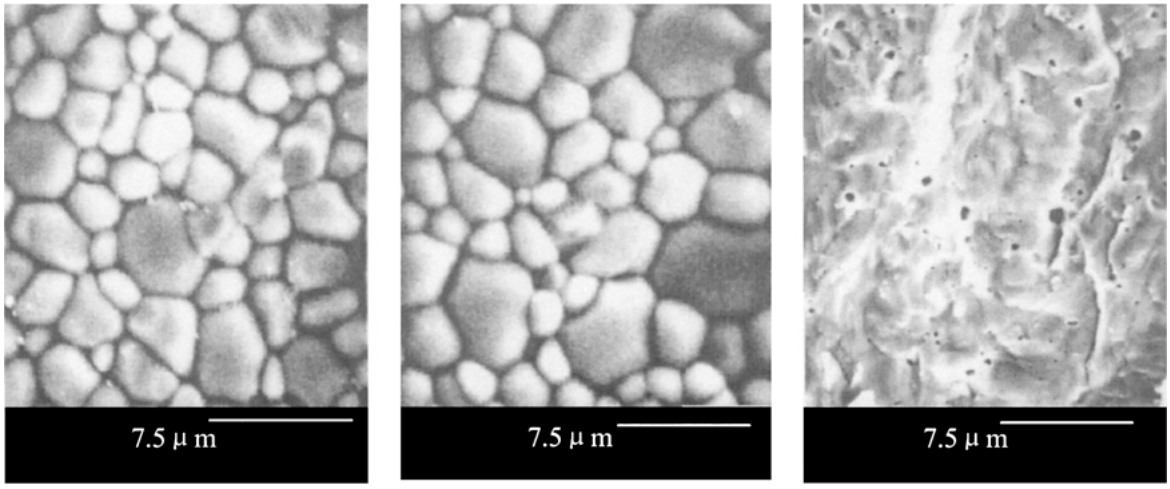

Figure 3 Microstructure of the surfaces (A and B) and fracture (C) of sintered LSGMn-1043 pellets before (A and C) and after (B) heat treatment in H_2 at 750°C for 5 h.

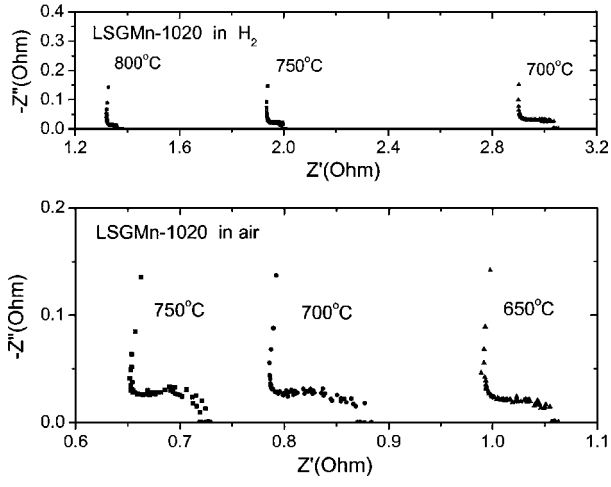

Figure 4 Typical impedance spectra of LSGMn-1020 in air and H_2 atmospheres.

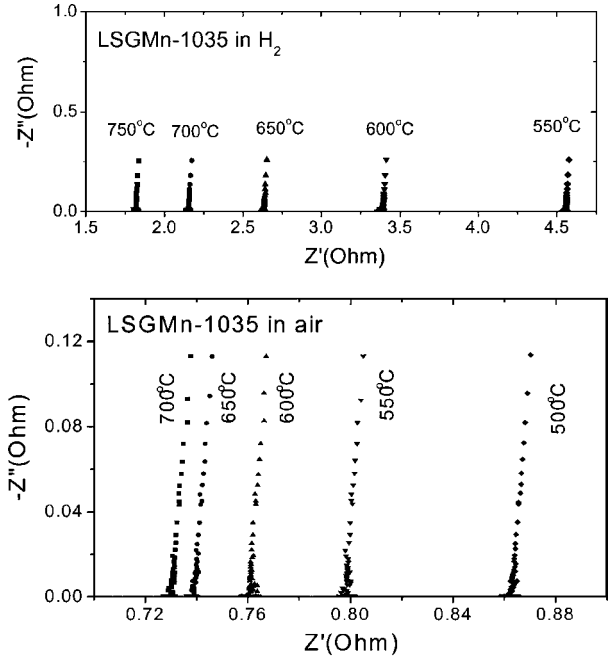

Figure 5 Typical impedance spectra of LSGMn-1035 in air and H_2 atmospheres.

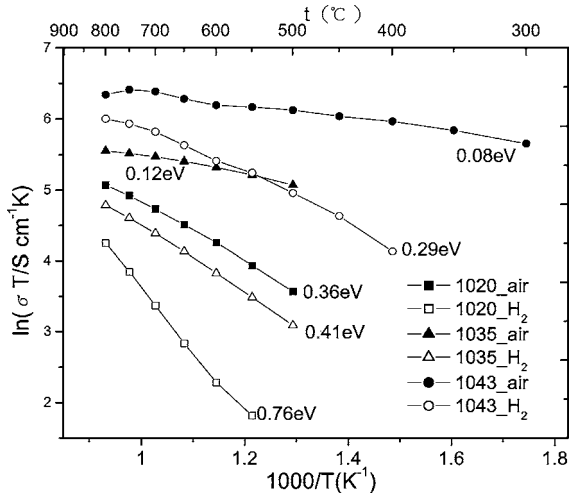

Figure 6 Temperature dependence of the conductivity of LSGMn doped with different amount of Mn in different atmospheres. The value adjacent each line is the activation energy for the electrical conduction in the material.

intercepts of the impedance spectra with the real-axis at high frequencies.

The temperature dependence of the electrical conductivity of LSGMn with different Mn content in H_2 and air was shown in Fig. 6. For clear data comparison, the conductivity at 600, 700 and 800°C as well as the apparent activation energy was also shown in Table I. It can be seen that the electrical conductivity in H_2 is lower than that in air. Generally, the transition metal doped lanthanum gallate exhibits p-type electronic conduction, and the mechanism of electronic transport is most likely to be hopping of p-type charge carriers [15]. Under reducing atmospheres, the following defect reaction may occur, which reduces the concentration of charge carriers-electronic holes, hence reduces the electrical conductivity.

$$O_O^{\times} + 2h^{\circ} = V_O^{\circ\circ} + \frac{1}{2}O_2 \qquad (2)$$

It can also be found that the activation energy in H_2 atmosphere is higher than that in air. This is

TABLE I Conductivity and activation energy for LSGMn doped with different amount of Mn in different atmospheres at 600,700 and 800°C

Composition	Atmosphere	Conductivity (S/cm) 600°C	700°C	800°C	Activation energy (eV)
LSGMn-1020	air	0.081	0.117	0.148	0.358
	H_2	0.011	0.030	0.065	0.758
LSGMn-1035	air	0.234	0.244	0.240	0.115
	H_2	0.053	0.083	0.112	0.407
LSGMn-1043	air	0.560	0.611	0.530	0.076
	H_2	0.256	0.346	0.377	0.288

because electronic conduction needs lower activation energy than ionic conduction, and in reducing atmospheres, ionic conduction becomes more dominating than in air, resulting in higher apparent activation energy.

As the Mn content increases, the conductivity in both air and H_2 is improved since more charge carriers are produced as more transition metal atoms are introduced into the lattice. When the transition metal dopant concentration exceeds a certain value, a 'percolation limit' (30–35%), electron transport even transfers from the p-type small polaron mechanism to metallic behavior [8]. In our work, for the sample LSGMn-1035 and LSGMn-1043, the conductivity in air at 800°C is lower than that at 700°C (see Table I), indicating these materials becomes metallic-like at high temperatures. The conductivity of LSGMn-1020, LSGMn-1035 and LSGMn-1043 in H_2 at 800°C is 0.065, 0.112 and 0.377 S/cm, respectively. Therefore, increasing the Mn content can effectively improve the electrical conductivity. So it is expected that the LSGMn anode with higher Mn content will have higher fuel cell performance, which will be discussed in Section 3.5.

3.4. Stability in reducing atmosphere

An important requirement for anode materials is good stability under reducing atmospheres. Fig. 7 shows the XRD patterns of sintered LSGMn pellets before and after heat treatment in H_2 at 750°C for 5 h. It can be seen that there is no apparent change after heat treatment in strong reducing atmosphere, indicating good phase stability for both lightly and heavily doped samples at least below 750°C, a suitable operating temperature for LSGM-based IT-SOFCs. Fig. 3B shows the surface microstructure of LSGMn-1043 sample after heat treatment in H_2. Compared with Fig. 3A, no apparent change was observed either. Therefore, we can conclude that the LSGMn materials with Mn contents investigated here are chemically stable at SOFC anode atmospheres at least below 750°C.

3.5. Fuel cell performance with LSGMn anodes

Fig. 8 shows the fuel cell performance with different anodes at 800°C. The three cells are the same except for the anodes, so the differences in fuel cell performance depend only on the anode performance. It can be clearly seen that the fuel cell with LSGMn-1043 anode has much higher performance than that with LSGMn-1020 anode, indicating improved performance of LSGMn-1043 over LSGMn-1020. This is partially due to the higher electrical conductivity of LSGMn-1043, as shown in Section 3.3. The higher conductivity will result in lower resistance polarization and hence higher performance. On the other hand, the dramatic performance improvement may strongly indicate the superior catalytic activity of LSGMn-1043 over LSGMn-1020 anodes toward the electrochemical oxidation of fuel. The peak power density reached 180 mW cm^{-2} at 800°C, despite the relative thick electrolyte

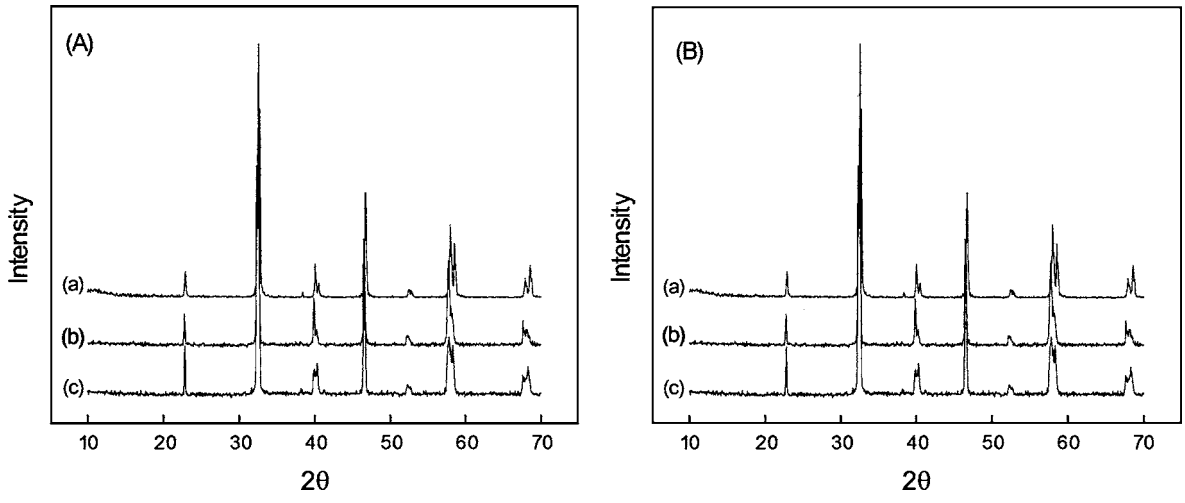

Figure 7 XRD patterns of sintered LSGMn pellets before (A) and after (B) heat treatment in H_2 at 750°C: (a) LSGMn-1020, (b) LSGMn-1035, and (c) LSGMn-1043.

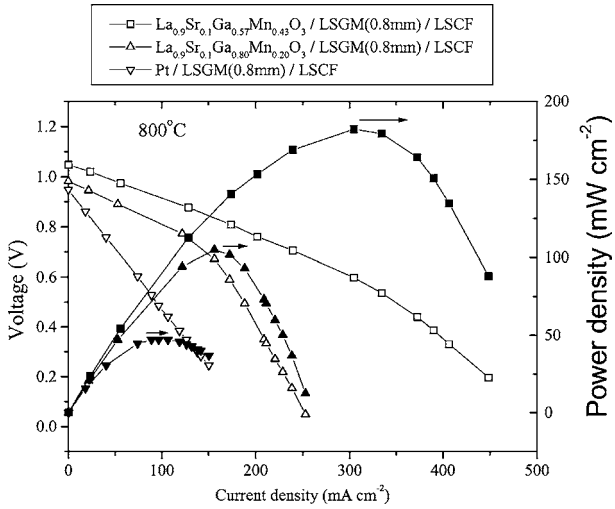

Figure 8 Comparison of fuel cell performance with different anode materials at 800°C.

(0.8 mm) here. In contrast, the fuel cell with Pt anode only showed a peak power density of 50 mW cm^{-2}. This may be due to the much less TPB area of Pt electrode than the mixed ionic/electronic conductive LSGMn anodes. It is expected that further performance improvement can be obtained by decreasing the electrolyte thickness or optimizing the microstructure of the LSGMn anodes.

4. Conclusions

Fine and homogeneous $La_{0.9}Sr_{0.1}Ga_{1-x}Mn_xO_{3-\delta}$ ($x = 0.20$, 0.35, 0.43) powders with high sinterability were synthesized by glycine-nitrate process. A single perovskite phase was formed after calcination at 1000°C for 4 h. The relative density of the sintered LSGMn pellets reaches 95% of theoretical value. Due to p-type electronic conduction mechanism, the electrical conductivity of LSGMn materials in H_2 atmosphere is lower than that in air. With increasing manganese content from 20 mol% to 43 mol%, the conductivity at 800°C in H_2 was increased by five-fold. Good chemical stability in H_2 at 750°C as well as relatively high conductivity makes them appropriate anode materials for Sr- and Mg-doped lanthanum gallate (LSGM)-based IT-SOFCs. Preliminary fuel cell measurement showed that LSGMn anode with higher Mn content exhibited far superior performance than that with lower Mn content, which may be partially due to the higher electrical conductivity. Although the LSGMn showed promising use as the LSGM-based fuel cell anode materials, further fuel cell performance improvement can be obtained by decreasing the electrolyte thickness or optimizing the anode microstructure.

Acknowledgements

The authors would like to thank the National Natural Science Foundation of China (Grant No. 20071029) and the Ministry of Science and Technology of China (Grant No G-2000026409 and 2001AA323090) for their financial support.

References

1. T. ISHIHARA, H. MATSUDA and Y. TAKITA, *J. Amer. Chem. Soc.* **116** (1994) 3801.
2. K. HUANG and J. B. GOODENOUGH, *J. Alloys and Compounds* **303/304** (2000) 454.
3. T. ISHIHARA, T. AKBAY, H. FURUTANI and Y. TAKITA, *Solid State Ionics* **113–115** (1998) 585.
4. T. ISHIHARA, T. YAMADA, T. AKBAY and Y. TAKITA, *Chem. Eng. Sci.* **54** (1999) 1535.
5. T. ISHIHARA, T. SHIBAYAMA, M. HONDA, H. NISHIGUCHI and Y. TAKITA, *J. Electrochem. Soc.* **147** (2000) 1332.
6. N. TROFIMENKO and H. ULLMANN, *Solid State Ionics* **124** (1999) 263.
7. *Idem.*, *ibid.* **118** (1999) 215.
8. V. V. KHARTON, A. P. VISKUP, A. A. YAREMCHENKO, R. T. BAKER, B. GHARBAGE, G. C. MATHER, F. M. FIGUEIREDO, E. N. NAUMOVICH and F. M. B. MARQUES, *ibid.* **132** (2000) 119.
9. F. L. CHEN and M. L. LIU, *J. Solid State Electrochem.* **3** (1998) 7.
10. X. G. ZHANG, S. OHARA, R. MARIC, H. OKAWA, T. FUKUI, H. YOSHIDA, T. INAGAKI and K. MIURA, *Solid State Ionics* **133** (2000) 153.
11. P. N. HUANG, A. HORKY and A. PETRIC, *J. Amer. Ceram. Soc.* **82**(9) (1999) 2402.
12. X. G. ZHANG, S. OHARA, R. MARIC, K. MUKAI, T. FUKUI, H. YOSHIDA, M. NISHIMURA, T. INAGAKI and K. MIURA, *Journal of Power Sources* **83** (1999) 170.
13. M. HROVAT, A. AHMAD-KHANLOU, Z. SAMARDZIJA and J. HOLC, *Mater. Res. Bull.* **34**(12/13) (1999) 2027.
14. B. C. H. STEELE, *Solid State Ionics* **86–88** (1996) 1223.
15. V. V. KHARTON, A. P. VISKUP, E. N. NAUMOVICH and N. M. LAPCHUK, *ibid.* **104** (1997) 67.
16. A. A. YAREMCHENKO, V. V. KHARTON, A. P. VISKUP, E. N. NAUMOVICH and N. M. LAPCHUK, *J. Solid State Chemistry* **142** (1999) 325.
17. A. A. YAREMCHENKO, V. V. KHARTON, A. P. VISKUP, E. N. NAUMOVICH, V. N. TIKHONOVICH and N. M. LAPCHUK, *Solid State Ionics* **120** (1999) 65.
18. Q. MING, M. D. NERSESYAN, A. WAGNER, J. RITCHIE, J. T. RICHARDSON, D. LUSS, A. J. JACOBSON and Y. L. YANG, *ibid.* **122** (1999) 113.
19. N. J. LONG, F. LECARPENTIER and H. L. TULLER, *Journal of Electroceramics* **3/4** (1999) 399.
20. H. ULLMANN and N. TROFIMENKO, *Solid State Ionics* **119** (1999) 1.
21. L. A. CHICK, L. R. PEDERSON, G. D. MAUPIN and J. L. BATES, *Mater. Lett.* **10** (1990) 6.
22. J. W. STEVENSON, T. R. ARMSTRONG, L. R. PEDERSON, J. LI, C. A. LEWINOHN and S. BASKARAN, *Solid State Ionics* **113–115** (1998) 571.

Received 31 July 2002
and accepted 21 January 2003